



## THERMAL PERFORMANCE OF SOLAR AIR HEATERS: MATHEMATICAL MODEL AND SOLUTION PROCEDURE

K. S. ONG

Faculty of Engineering, University of Malaya, Pantai Valley, 59100 Kuala Lumpur, Malaysia

(Communicated by Associate Editor BRIAN NORTON)

**Abstract**—A mathematical model and solution procedure for predicting the thermal performance of single-pass solar air collectors is presented. By omitting or providing a top glass cover over a plane absorber plate, or by providing a bottom plate under the absorber plate and circulating air over one or both of the air channels so formed, four common types of flat-plate solar air collector designs were considered. The surface temperatures of the walls surrounding the air streams were assumed uniform whereas the air temperatures were assumed to vary linearly along the collector. In the mathematical model, the solar collector was assumed sufficiently short for which the assumptions were valid. By considering a steady state heat transfer using the thermal network analysis procedure, a set of simultaneous equations for the mean temperature of the walls and the air streams were obtained. Instead of solving the simultaneous equations for mean temperatures explicitly, a matrix inversion method was employed using a standard sub-routine programme. Because heat transfer coefficients were temperature dependent, a set of mean temperatures was approximated which allowed the heat transfer coefficients to be evaluated as a first guess. An iterative process was then created that enabled the mean temperatures for the collector to be calculated. The newly-calculated mean temperatures were then compared with the initially-guessed temperatures. The iterative procedure was repeated until consecutive mean temperature values differed by less than  $0.01^{\circ}\text{C}$ . After this, another section of collector with a length equal to the previous one was added to the end of the first collector. The temperature conditions at the inlet of the second section were assumed equal to the outlet temperature conditions of the previous section. The iterative procedure to determine the mean temperatures was repeated for the next section. Additional sections were added until the required overall length of collector was considered. By this procedure, predictions of mean wall and air streams temperatures for a collector of any length could be obtained. Although only four, common single-pass types of flat-plate solar collectors are considered here, the solution procedure could be extended to encompass most other collector designs.

### 1. INTRODUCTION

A solar air heater system consists of an array of interconnected solar heat collectors. Most systems incorporate a once-through or single-pass type of forced air circulation with cold ambient air intake and solar-heated hot air discharge to the working space. The collectors may be connected in series, parallel, or a series-parallel combination. A series-only connection would result in a long but higher temperature system whereas a parallel-only connection would result in a short but lower temperature system. Apart from the length effect, the performance of the system would also depend upon the air circulation rate, physical design of the collectors, and prevailing ambient conditions. Therefore, a knowledge of the operating characteristics of the collectors would enable the system performance to be optimised.

There are numerous works on both experimental and theoretical performance of solar air heaters. Recent works by Parker (1981), Vijeyndera *et al.* (1982), Than and Ong (1984), Biondi *et al.* (1988), Duffie and Beckman

(1991), Verma *et al.* (1992), and Parker *et al.* (1993) considered the steady state heat balance equations and involved linking plate efficiency and heat removal factors with air flow rates, surface wind heat transfer coefficients, and heat transfer coefficients between the moving air streams and the surfaces forming the flow channels. The derivation of these factors are quite complex and require considerable effort especially when dealing with the numerous design configurations available involving different combinations of geometrical details and air flow patterns.

### 2. OBJECTIVE

The following types of flat-plate solar air collectors are shown in Fig. 1: Type (I)—Single channel design with single air flow between top glass and bottom absorber plate; Type (II)—Single channel design with single air flow between absorber and bottom plates (no glass); Type (III)—Double channel design with single air flow between absorber and bottom plates; Type (IV)—Double channel design with double

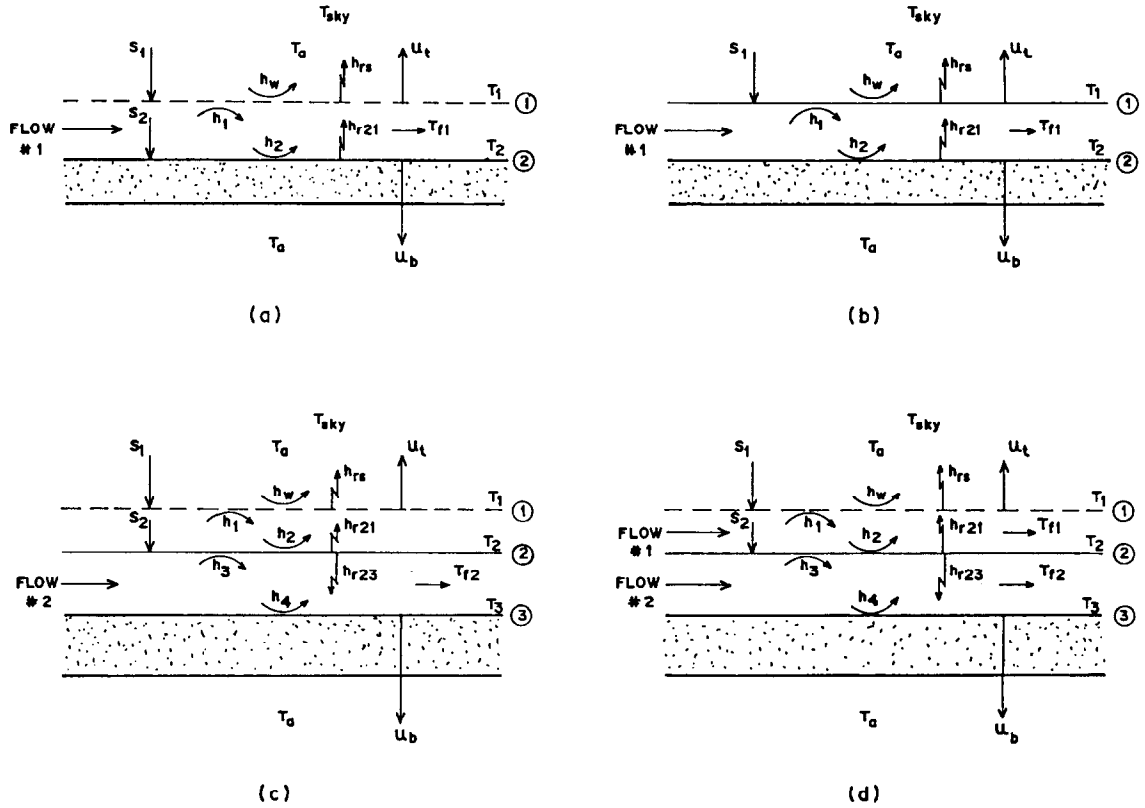


Fig. 1. The basic solar air collector types: (a) Type I, (b) Type II, (c) Type III, and (d) Type IV.

air flows between top glass and absorber plate and between absorber and bottom plates. In all the designs, the absorber plate is black-painted over the top surface and the bottom of the collector could be insulated or left bare.

### 3. ANALYSIS

#### 3.1. Thermal network

The thermal networks for the four types of solar collectors considered are shown in Fig. 2. For Type (IV), the following heat balance equations are obtained from the thermal network at the points:

$$T_1: S_1 + h_{r21}(T_2 - T_1) + h_1(T_{f1} - T_1) = U_t(T_1 - T_a) \quad (1)$$

$$T_{f1}: h_2(T_2 - T_{f1}) = h_1(T_{f1} - T_1) + Q_1 \quad (2)$$

$$T_2: S_2 = h_3(T_2 - T_{f2}) + h_2(T_2 - T_{f1}) + h_{r23}(T_2 - T_3) + h_{r21}(T_2 - T_1) \quad (3)$$

$$T_{f2}: h_3(T_2 - T_{f2}) = h_4(T_{f2} - T_3) + Q_2 \quad \text{and} \quad (4)$$

$$T_3: h_4(T_{f2} - T_3) + h_{r23}(T_2 - T_3) = U_b(T_3 - T_a) \quad (5)$$

For Types (I) and (II), eqns (4) and (5) are not valid and the heat balance eqn (3) is replaced by the following equation at the point:

$$T_2: S_2 = h_2(T_2 - T_{f1}) + h_{r21}(T_2 - T_1) + U_b(T_2 - T_a) \quad (6)$$

For Type (II), the absorber surface is non-transparent and hence there is no transfer of solar radiation to the bottom plate, viz.,  $S_2$  equals zero. In this case, the heat balance eqn (6) is replaced by the following equation at the point:

$$T_2: 0 = h_2(T_2 - T_{f1}) + h_{r21}(T_2 - T_1) + U_b(T_2 - T_a) \quad (7)$$

For Type (III), there is no heat extracted from the system between the top cover and the stagnant air cavity. The air is assumed to recirculate within the space under free convection in an inclined wall cavity. Hence eqn (2) does not

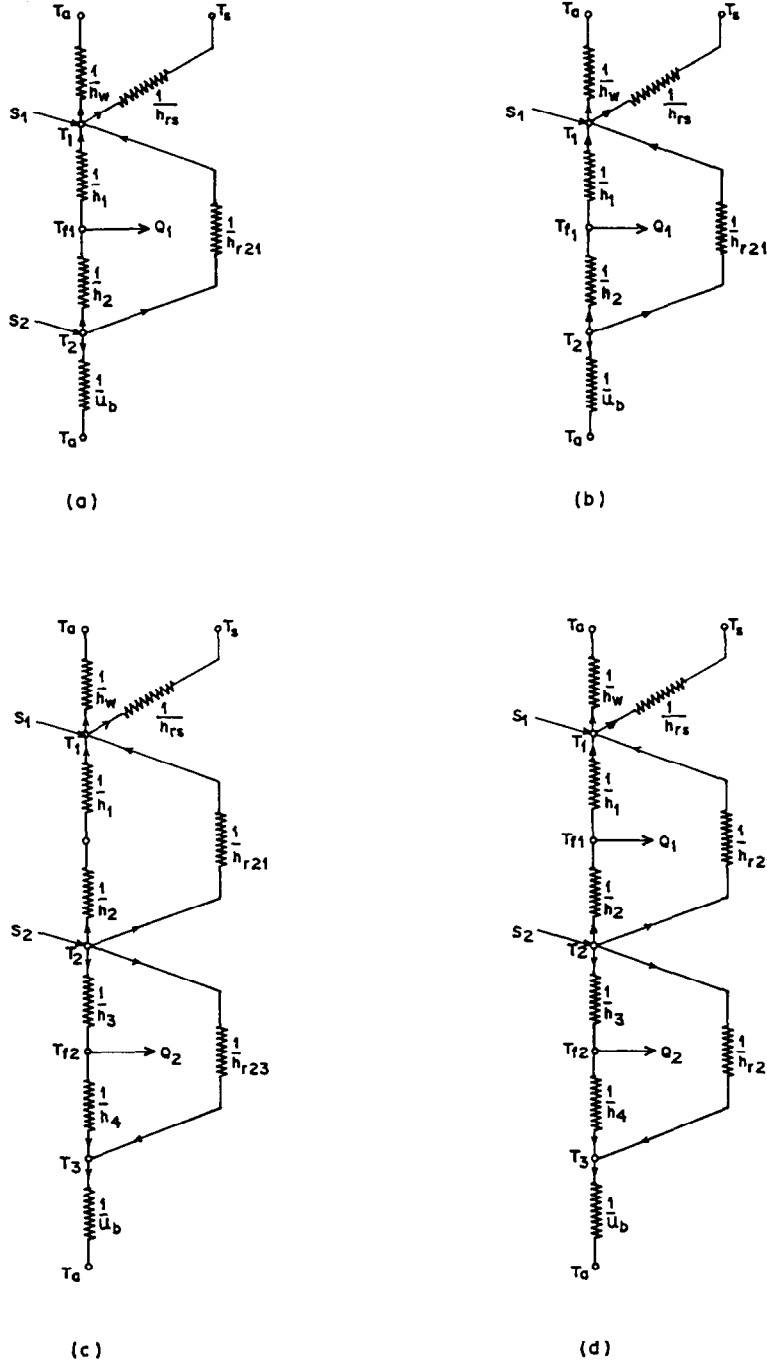


Fig. 2. Thermal network for solar air collectors: (a) Type I, (b) Type II, (c) Type III, and (d) Type IV.

exist and eqns (1) and (3) are replaced by the following at the points:

$$T_1: S_1 + h_{r21}(T_2 - T_1) + h_{nc}(T_2 - T_1) = U_t(T_1 - T_a) \quad \text{and} \quad (8)$$

$$T_2: S_2 = h_3(T_2 - T_{f2}) + h_{nc}(T_2 - T_1) + h_{r23}(T_2 - T_3) + h_{r21}(T_2 - T_1) \quad (9)$$

### 3.2. Temperature distribution along flow direction

Consider the heat flows into and out of an element of thickness  $\delta y$  in a single air stream at a distance  $y$  from the entrance of a collector as shown in Fig. 3. The temperatures of the walls of the duct forming the air channel are assumed uniform but not equal to each other for each

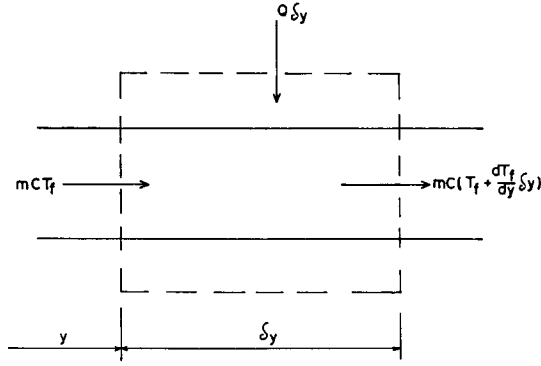


Fig. 3. Heat balance on element along flow direction.

wall. The temperature of the air stream at a distance  $y$  from the collector inlet is assumed to be at  $T_f$ . The temperature is assumed uniform throughout the cross section. At the outlet of the section ( $y + \delta y$ ), the mean air temperature is equal to  $[T_f + (dT_f/dy) \delta y]$ . The heat balance for the element is thus

$$mC T_f + QW \delta y = mC \left( T_f + \frac{dT_f}{dy} \delta y \right) \quad (10)$$

Simplifying and dividing by  $\delta y$  we obtain

$$dT_f/dy = QW/(mC) \quad (11)$$

By assuming that the useful heat transferred to the air is uniform along a collector of length  $L$ , the mean air temperature at the outlet can be found by integrating the above equation to give

$$T_{f,o} - T_{f,i} = QWL/(mC) \quad (12)$$

This assumption implies that the air temperature varies linearly along the collector as shown in Fig. 4. From observations, this assumption is valid for "short" collectors. The mean air temperature is then equal to the arithmetic mean

$$T_f = (T_{f,i} + T_{f,o})/2 \quad (13)$$

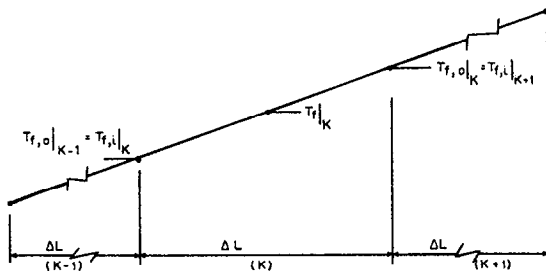


Fig. 4. Linear fluid temperature variation along collector.

The useful heat transferred to the moving air stream can then be written in terms of the mean fluid and inlet temperatures as

$$Q = 2mC(T_f - T_{f,i})/(WL) \quad (14)$$

For the case of the two-channel flow assumed, where the two streams are at the mean air temperatures  $T_{f1}$  and  $T_{f2}$ :

$$Q_1 = 2m_1 C(T_{f1} - T_{f1,i})/(WL) \quad \text{and} \quad (15)$$

$$Q_2 = 2m_2 C(T_{f2} - T_{f2,i})/(WL) \quad (16)$$

By introducing  $\Gamma_1 = 2m_1 C/(WL)$ , and  $\Gamma_2 = 2m_2 C/(WL)$  into the above,  $Q_1$  and  $Q_2$  may be expressed as:

$$Q_1 = \Gamma_1(T_{f1} - T_{f1,i}) \quad \text{and} \quad (17)$$

$$Q_2 = \Gamma_2(T_{f2} - T_{f2,i}) \quad (18)$$

### 3.3. Mean temperatures matrices

By substituting eqns (17) and (18) into eqns (2) and (4) and rearranging we obtain the following expressions for the Type (IV) collector

$$(h_1 + h_{r21} + U_t)T_1 - h_1 T_{f1} - h_{r21} T_2 = S_1 + U_t T_a \quad (19)$$

$$h_1 T_1 - (h_1 + h_2 + \Gamma_1)T_{f1} + h_2 T_2 = -\Gamma_1 T_{f1,i} \quad (20)$$

$$-h_{r21} T_1 - h_2 T_{f1} + (h_2 + h_3 + h_{r21} + h_{r23})T_2 - h_3 T_{f2} - h_{r23} T_3 = S_2 \quad (21)$$

$$h_3 T_2 - (h_3 + h_4 + \Gamma_2)T_{f2} + h_4 T_3 = -\Gamma_2 T_{f2,i} \quad \text{and} \quad (22)$$

$$-h_{r23} T_2 - h_4 T_{f2} + (h_{r23} + U_b + h_4)T_3 = U_b T_a \quad (23)$$

For Types (I) and (II), eqns (22) and (23) are not valid and eqn (21) is replaced by

$$-h_{r21} T_1 - h_2 T_{f1} + (h_2 + h_{r21} + U_b)T_2 = S_2 + U_b T_a \quad (24)$$

Further, for Type (II), the term  $S_2$  in eqn (24) equals zero.

For Type (III), eqn (20) is not valid and eqns (19) and (21) are replaced by

$$(h_{nc} + h_{r21} + U_t)T_1 - (h_{nc} + h_{r21})T_2 = S_1 + U_t T_a \quad (25)$$

$$-(h_{r21} + h_{nc})T_1 + (h_{nc} + h_3 + h_{r21} + h_{r23})T_2 - h_3 T_{f2} - h_{r23} T_3 = S_2 \quad (26)$$

In general, the above eqns (19)–(26) may be displayed in a  $5 \times 5$  matrix form:

$$\begin{bmatrix} (h_1 + h_{r21} + U_t) & -h_1 & -h_{r21} & 0 & 0 \\ h_1 & -(h_1 + h_2 + \Gamma_1) & h_2 & 0 & 0 \\ -h_{r21} & -h_2 & (h_2 + h_3 + h_{r21} + h_{r23}) & -h_3 & -h_{r23} \\ 0 & 0 & h_3 & -(h_3 + h_4 + \Gamma_2) & h_4 \\ 0 & 0 & -h_{r23} & -h_4 & (h_{r23} + U_b + h_4) \end{bmatrix} \begin{bmatrix} T_1 \\ T_{f1} \\ T_2 \\ T_{f2} \\ T_3 \end{bmatrix} = \begin{bmatrix} U_t T_a + S_1 \\ -\Gamma_1 T_{f1,i} \\ S_2 \\ -\Gamma_2 T_{f2,i} \\ U_b T_a \end{bmatrix}$$

For Type (III) the equivalent matrix is  $4 \times 4$ :

$$\begin{bmatrix} (h_{nc} + h_{r21} + U_t) & (h_{nc} + h_{r21}) & 0 & 0 \\ -(h_{nc} + h_{r21}) & (h_{nc} + h_3 + h_{r21} + h_{r23}) & -h_3 & -h_{r23} \\ 0 & h_3 & -(h_3 + h_4 + \Gamma_2) & h_4 \\ 0 & -h_{r23} & -h_4 & (h_{r23} + U_b + h_4) \end{bmatrix} \begin{bmatrix} T_1 \\ T_2 \\ T_{f2} \\ T_3 \end{bmatrix} = \begin{bmatrix} U_t T_a + S_1 \\ S_2 \\ -\Gamma_2 T_{f2,i} \\ U_b T_a \end{bmatrix}$$

For Types (I) and (II) the equivalent  $3 \times 3$  matrices are:

$$\begin{bmatrix} (h_1 + h_{r21} + U_t) & -h_1 & -h_{r21} \\ h_1 & -(h_1 + h_2 + \Gamma_1) & h_2 \\ -h_{r21} & -h_2 & (h_2 + h_{r21} + U_b) \end{bmatrix} \begin{bmatrix} T_1 \\ T_{f1} \\ T_2 \end{bmatrix} = \begin{bmatrix} U_t T_a + S_1 \\ -\Gamma_1 T_{f1,i} \\ S_2 + U_b T_a \end{bmatrix}$$

Further, for Type (II),  $S_2$  equals zero. In general, the above matrices may be displayed as

$$[\mathbf{A}][\mathbf{T}] = [\mathbf{B}] \quad (27)$$

The mean temperature vector may be determined by matrix inversion using standard computer packages

$$[\mathbf{T}] = [\mathbf{A}]^{-1}[\mathbf{B}] \quad (28)$$

### 3.4. Radiation heat transfer coefficients from top and bottom surfaces

The radiation heat transfer coefficient from the top surface to the sky referred to the ambient temperature can be written as

$$h_{rs} = \sigma \epsilon_1 (T_1 + T_s)(T_1^2 + T_s^2)(T_1 - T_s)/(T_1 - T_a) \quad (29)$$

The sky temperature obtained from Swinbank (1963) is given by

$$T_s = 0.0552 T_a^{1.5} \quad (30)$$

### 3.5. Convection heat transfer from cover due to wind

The convection heat transfer coefficient due to wind from McAdams (1954):

$$h_w = 5.7 + 3.8 V \quad (31)$$

Watmuff *et al.* (1977) give this equation as:

$$h_w = 2.8 + 3.3 V \quad (32)$$

The wind coefficient could also be determined from the correlation developed by Sparrow *et al.* (1979):

$$Nu_w = 0.0158 Re^{0.8} \quad (33)$$

where the Reynolds number is calculated based on the equivalent diameter  $D_h$  equal to  $4 \times$  plate area/plate perimeter.

Table 1 shows values of wind coefficients calculated from the correlations presented by McAdams (1954), Watmuff *et al.* (1977), and Sparrow *et al.* (1979). Generally, the values

Table 1. Wind coefficients,  $h_w$  ( $\text{W m}^{-2} \text{K}^{-1}$ )

	Wind velocity $V$ ( $\text{m s}^{-1}$ )				
	0.0	0.5	1.0	2.0	3.0
McAdams (1954)	5.7	7.6	9.5	13.3	17.1
Watmuff <i>et al.</i> (1977)	2.8	4.3	5.8	8.8	11.8
Sparrow <i>et al.</i> (1979)	0.0	3.0	4.2	6.0	7.3

obtained using McAdams' correlation was roughly twice that given by the other two correlations. Unless otherwise stated, McAdam's correlation will be employed in this article.

### 3.6. Radiation heat transfer between parallel plates

The radiation heat transfer coefficients between two infinite parallel plates set 1-2 and 2-3 are given as

$$h_{r21} = \sigma(T_1^2 + T_2^2)(T_1 + T_2)/(1/\epsilon_1 + 1/\epsilon_2 - 1) \quad (34)$$

and

$$h_{r23} = \sigma(T_3^2 + T_2^2)(T_3 + T_2)/(1/\epsilon_3 + 1/\epsilon_4 - 1) \quad (35)$$

### 3.7. Forced convection heat transfer coefficient between parallel plates

**3.7.1. Laminar flow region ( $Re < 2300$ ).** Heaton *et al.* (1964) proposed the following empirical correlation for the local Nusselt number for laminar flow between two parallel flat plates with one side insulated and the other subjected to a constant heat flux:

$$Nu = Nu_\infty + \frac{a[Re Pr(D_h/L)]^m}{1 + b[Re Pr(D_h/L)]^n} \quad (36)$$

where the constants are  $a = 0.00190$ ,  $b = 0.00563$ ,  $m = 1.71$ ,  $n = 1.17$ , and  $Nu_\infty = 5.4$  for  $Pr = 0.7$ .

**3.7.2. Transition flow region ( $2300 < Re < 6000$ ).** Hausen (1943) presented the following empirical correlation for the average Nusselt number between the beginning of the heated section and the position  $L$  for flow in a tube:

$$Nu = 0.116(Re^{2/3} - 125) Pr^{1/3} \times [1 + (D_h/L)^{2/3}](\mu/\mu_w)^{0.14} \quad (37)$$

**3.7.3. Turbulent flow region ( $Re > 6000$ ).** Tan and Charters (1970) recommended that for flat-plate solar air heaters, the heat transfer in the developed flow region should be obtained from the relationship:

$$Nu_\infty = 0.018 Re^{0.8} Pr^{0.4} \quad (38)$$

for  $9500 < Re < 22,000$ .

For situations involving a large property variation, the Sieder and Tate (1936) equation may be employed

$$Nu = 0.027 Re^{0.8} Pr^{1/3} (\mu/\mu_w)^{0.14} \quad (39)$$

for flow in smooth pipes where  $Re > 10,000$  and  $L/D > 60$ .

A more accurate correlation which is also applicable for rough ducts was developed by Petukhov (1970)

$$Nu = (Re Pr/X)(f/8)(\mu/\mu_w)^n \quad (40)$$

where, for  $10^4 < Re < 5 \times 10^6$ ,  $X = 1.07 + 12.7(Pr^{2/3} - 1)(f/8)^{1/2}$ ;  $n = 0.11$  (heating with uniform  $T_w$ ),  $n = 0.25$  (cooling with uniform  $T_w$ ), and  $n = 0$  (uniform wall heat flux or gases).

The friction factor for smooth tubes for the above equation may be obtained from

$$f = [1.82 \log(Re) - 1.64]^{-2} \quad (41)$$

**3.7.4. Entrance region ( $L/D < 60$ ).** In the entrance region, greater heat transfer coefficients may be expected. In their studies on the effect of the thermal entrance region on turbulent, forced convective heat transfer for an asymmetrically heated, rectangular duct with uniform heating, Tan and Charters (1969) determined an expression for the mean Nusselt Number

$$Nu = Nu_\infty(1 + SD_h/L) \quad (42)$$

where the factor  $S$  was found to be adequately represented by

$$3.57 < L/D_h \leq 60: S = 14.3 \log(L/D_h) - 7.9 \quad (43)$$

$$L/D_h > 60: S = 17.53 \quad (44)$$

It should be noted here that  $S$  is 0 when  $L/D_h$  equals 3.57. The range of Reynolds Numbers covered in their studies was from 9500 to 22,000. Nusselt (1931) recommended the use of

$$Nu = 0.036 Re^{0.8} Pr^{1/3} (D/L)^{0.055} \quad (45)$$

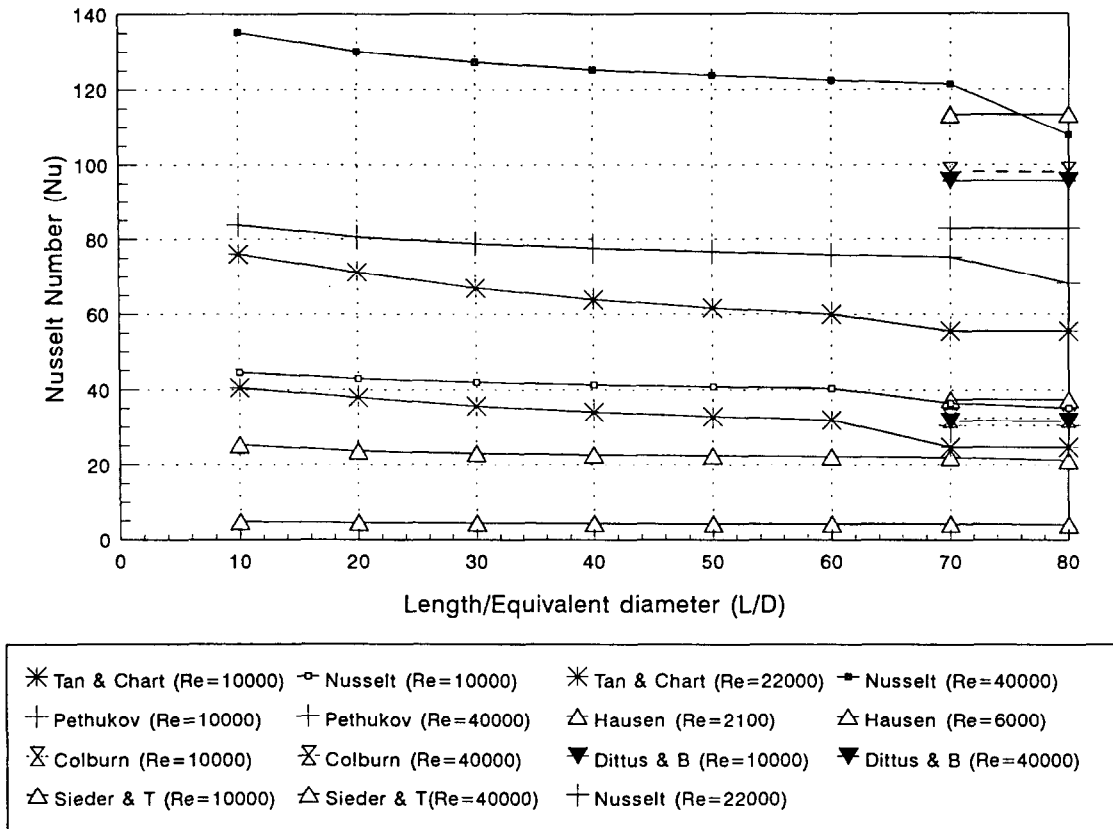
in the entrance region for  $10 < L/D < 400$ .

For noncircular ducts, the tube diameter is replaced by the hydraulic or equivalent diameter defined as

$$D_h = 4A_c/P \quad (46)$$

For flows in between parallel flat plates, the equivalent diameter  $D_e$  is twice the separation distance between the plates.

Figure 5 shows the Nusselt Numbers

Fig. 5. Nusselt Number versus  $L/D$ .

obtained from the above empirical correlations for comparison. A discontinuity in the curve can be observed in the Tan and Charters (1969) correlations at  $L/D > 60$  because of the maximum value of  $S$  imposed. As a result, this correlation is not convenient to use in the present work. It is better to use Nusselt's (1931) correlation in the entry region because the equation takes the entry length into account without any discontinuity in evaluating the Nusselt Number. The values obtained using Nusselt's correlation are higher than those given by the other correlations. By comparing the Nusselt numbers in the fully developed region ( $L/D > 60$ ) for turbulent flow, the ratios of Nusselt Numbers from Tan and Charters/Nusselt and from Petukhov/Nusselt correlations are obtained and tabulated in Table 2.

Differences can be expected in the Nusselt Number depending upon which correlation is employed. The variation may range from  $\pm 50\%$ . In the present work, the heat transfer coefficient correlations as listed in Table 3 will be assumed. These correlations will be employed pending better ones in order to demonstrate the qualitative accuracy of the theoretical model employed to simulate the thermal performances of the different types of solar air heaters.

### 3.8. Natural convection between parallel plates

Hollands *et al.* (1976) gives the following relationship between the Nusselt Number and Rayleigh Number for free convection between inclined planes lying in the range  $0 < Ra < 10^5$

Table 2. Ratio of Nusselt Numbers

	Ratio of Nusselt Number		
	Re = 10,000	Re = 22,000	Re = 40,000
Tan and Charters (1969): Nusselt (1931)	0.79	0.79	
Petukhov (1970): Nusselt (1931)	0.75		0.68

Table 3. List of correlations employed for forced convection HTC

Flow Regime	Range of Re	Equation
Laminar flow	$Re \leq 2,100$	Heaton <i>et al.</i> (1964), eqn (36)
Transition flow	$2,100 < Re < 10,000$	Hausen (1943), eqn (37)
Turbulent flow	$10,000 \leq Re$	Nusselt (1931), eqn (45)

and  $0^\circ \leq \phi \leq 60^\circ$ :

$$Nu_{nc} = 1 + 1.44 \left[ 1 - \frac{1708 (\sin 1.8 \phi)^{1.6}}{Ra \cos \phi} \right] \left[ 1 - \frac{1708}{Ra \cos \phi} \right]^+ + \left[ \left( \frac{Ra \cos \phi}{5830} \right)^{1/3} - 1 \right]^+ \quad (47)$$

The equivalent diameter employed in the above definition for the Nusselt Number is the separation distance between the plates. Also, the notation  $[ ]^+$  is used to denote that if the quantity in the bracket is negative, it should be set equal to zero. The natural convection coefficient is specified for Type (III) for the air cavity between the glass and absorber surfaces.

### 3.9. Overall top heat transfer coefficient

The overall top heat loss coefficient may be obtained from

$$U_t = h_w + h_{rs} \quad (48)$$

### 3.10. Conduction heat transfer from bottom surface

The bottom heat loss coefficient is given by

$$U_b = \frac{1}{\sum_{i=1}^n (x_{bi}/k_{bi}) + 1/h_w} \quad (49)$$

In the absence of bottom insulation, the insulation thicknesses are set equal to zero.

### 3.11. Solar radiation

The solar radiation heat flux absorbed by the first surface is

$$S_1 = \alpha_1 H \quad (50)$$

and the solar radiation heat flux absorbed by the second surface is

$$S_2 = \tau \alpha_2 H \quad (51)$$

For Type (II),  $S_2$  equals zero because  $\tau$  for a solid absorber surface is equal to zero.

### 3.12. Instantaneous efficiency

The instantaneous heat collection efficiency of the first air stream for a collector of length  $L$

is defined as

$$\cap_1 = m_1 C(T_{f1,o} - T_a)/(HWL) \quad (52)$$

and for the second air stream, if it exists, is

$$\cap_2 = m_2 C(T_{f2,o} - T_a)/(HWL) \quad (53)$$

In the above equations, the inlet air temperatures are assumed to be at ambient. For the Type (IV) collector, the combined instantaneous heat collection efficiency of both the air streams is obtained by adding the individual air stream efficiencies

$$\cap_0 = \cap_1 + \cap_2 \quad (54)$$

The theoretical model assumes that air temperatures vary linearly over short collectors. Instantaneous efficiencies are expected to decrease as the length of the collector increases.

### 3.13. Physical properties

The physical properties of air are assumed to vary linearly with temperature  $T^\circ\text{C}$  because of the low temperature range to be encountered. The following are assumed for:

viscosity

$$\mu = [1.983 + 0.00184(T - 27)] 10^{-5} \quad (55)$$

density

$$\rho = 1.1774 - 0.00359(T - 27) \quad (56)$$

thermal conductivity

$$k = 0.02624 + 0.0000758(T - 27) \quad (57)$$

specific heat

$$C = 1.0057 + 0.000066(T - 27) \quad (58)$$

## 4. THEORETICAL SOLUTION PROCEDURE

The theoretical model assumes that for a short collector, the temperatures of the walls surrounding the air streams are uniform and the temperatures of the air streams vary linearly along the collector. A long collector can be assumed to be divided equally into a finite number of short collectors, or sections. The wall and mean air temperatures of the first section are initially guessed and specified. In all cases, they are set equal to the ambient temperature.

Heat transfer coefficients are evaluated according to the initially-guessed temperature values. An iterative process is then created and the mean temperatures for the section calculated using the equations derived by employing a standard package matrix-inversion subroutine. The newly-calculated temperature values are then compared with the previously assumed ones. The iterative process is repeated until all consecutive mean temperatures differ by less than  $0.01^{\circ}\text{C}$ .

Another section of collector, with length equal to the previous section, was added to the end of the first section. The mean wall and air temperatures of the second section of collector are then set equal to the mean wall and air temperatures of the section before it. The inlet air temperature of the second section is set equal to the outlet air temperature of the first section. The iterative procedure is repeated until all the sections of the given collector are considered. By this procedure, wall and mean air temperatures can be predicted for the complete length of collector.

The computer programme, based on

FORTRAN, is outlined in the Flowchart shown in Fig. 6. The start of the programme considers the first section. An initial guess of the mean wall temperatures and mean air streams temperatures are made. For the first section, these temperatures are specified equal to ambient temperature. (For subsequent sections, the initial temperatures are specified equal to the respective temperature values of the respective previous sections.) An iterative process is then initiated. The programme calculates all the required heat transfer and heat loss coefficients based on the initially-guessed temperatures. The matrices  $[A]$ ,  $[T]$ , and  $[B]$  are then set up. A standard matrix inversion subroutine is then called to invert  $[A]^{-1}$  to determine a new set of temperature matrix  $[T']$ . Each new temperature value in the matrix  $[T']$  is then compared with the corresponding initially-guessed  $[T]$ . If the difference between any corresponding new and old values exceeds  $0.01^{\circ}\text{C}$ , the iteration is stopped and the old temperatures are then replaced with the newly-calculated ones and taken to be the required temperatures at the section concerned. At the end of the iteration,

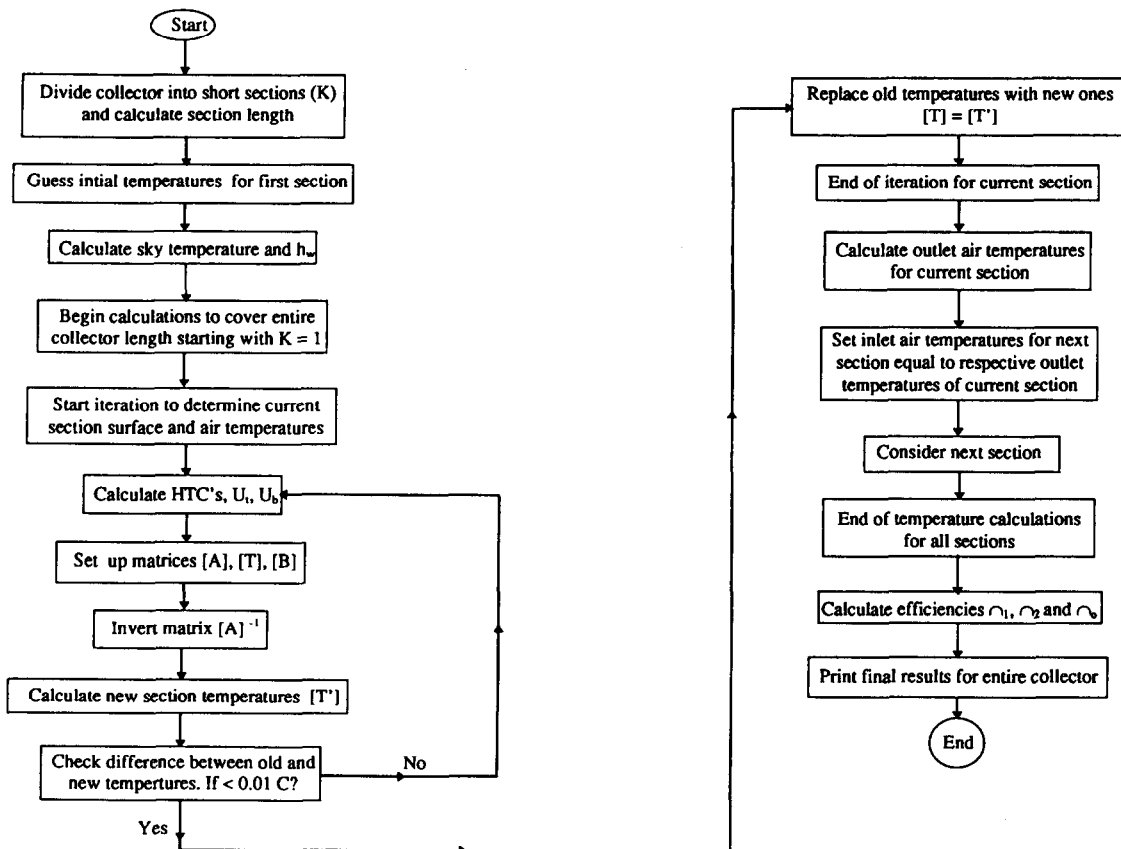


Fig. 6. Flowchart for computer programme.

the programme calculates the outlet temperatures of the two air streams and also the efficiencies at the end of the current section. It then sets the air temperatures at the inlet of the next section equal to the outlet air temperatures of the current section.

The programme then proceeds to look at the next section. The iterative solution procedure to determine the new mean temperatures of this next section is then repeated. By this repetitive and iterative process, the required temperatures along the entire length of the solar heater could be obtained, section by section. Normally, the number of iterations required is not more than two or three.

## 5. THEORETICAL PREDICTION

Values of absorptivity, emissivity, and transmissivity for the various surfaces are assumed values taken from generally accepted figures and not measured values. From preliminary results, it was seen that small temperature differences of the order of  $1^{\circ}\text{C}$  or less could be obtained by modifying these values. This meant that the prediction was not heavily dependent upon these values. The mathematical model allows for different values of heat transfer coefficients to be specified for the upper and lower surfaces of the walls forming the air channels. In the present programme, the coefficients for both upper and lower surfaces of each channel were assumed equal,  $h_1 = h_2$  and  $h_3 = h_4$ .

### 5.1. Effects of section size

As stated earlier, the theoretical model assumes that for a short collector, the wall temperatures are assumed uniform and the air temperatures are assumed to vary linearly along the collector in the direction of flow. From observations, these assumptions are valid for short collectors. However, for a long collector,

the temperature rise is expected to be asymptotic. In order to determine the effect of section length, three different sets of predicted temperature results were obtained and compared, each with a different value of section length. It was observed that plate temperatures differed by less than  $0.5^{\circ}\text{C}$  between the results obtained for 0.5 m and 1.0 m sections. Also, the air temperatures and efficiency values remained nearly the same for these two sets. Hence, for the present purpose it could be deemed that satisfactory results could be obtained by using a 1 m section collector.

### 5.2. Temperature variation along flow direction

Predictions were obtained for the four types of collectors considered by assuming air mass flow rates equal to 0.04 and  $0.40\text{ kg s}^{-1}$  for the ambient conditions assumed according to Table 4. For discussion purposes, the Reynolds Numbers based on these flow rates are evaluated at  $27^{\circ}\text{C}$  and are equal to 4000 and 40,000.

Wall and air stream temperatures are shown plotted in Figs 7–14 for the four different types of collectors at Reynolds Numbers of 4000 and 40,000. These correspond to flows in the usually encountered transition and turbulent flow regimes. It can be seen that, as expected, as air flow rate increases, temperature decreases. Also, for high flow rates the collector operating temperature would be lower, thus resulting in higher efficiencies. In all the results, it was observed that the absorber plate exhibited the highest temperature, and the glass the lowest. As air flow rate increases, the temperature differences between the air stream and the glass bottom plate decrease.

### 5.3. Effects of wind convective heat transfer coefficient

A typical value of radiation heat transfer coefficient from the top surface of a collector at  $100^{\circ}\text{C}$  and ambient at  $27^{\circ}\text{C}$  from eqn (29) is

Table 4. List of parameters assumed in predictions

Collector type	Radiation intensity $H\text{ (W m}^{-2}\text{)}$	Ambient temperature $T_a\text{ (}^{\circ}\text{C)}$	Wind velocity $V\text{ (m s}^{-1}\text{)}$	Air flowrate stream #1 $m_1\text{ (kg s}^{-1}\text{)}$	Air flowrate stream #2 $m_2\text{ (kg s}^{-1}\text{)}$
1	700	27	1.0	0.04	0.00
1	700	27	1.0	0.40	0.00
2	700	27	1.0	0.04	0.00
2	700	27	1.0	0.40	0.00
3	700	27	1.0	0.00	0.04
3	700	27	1.0	0.00	0.40
4	700	27	1.0	0.04	0.04
4	700	27	1.0	0.40	0.40

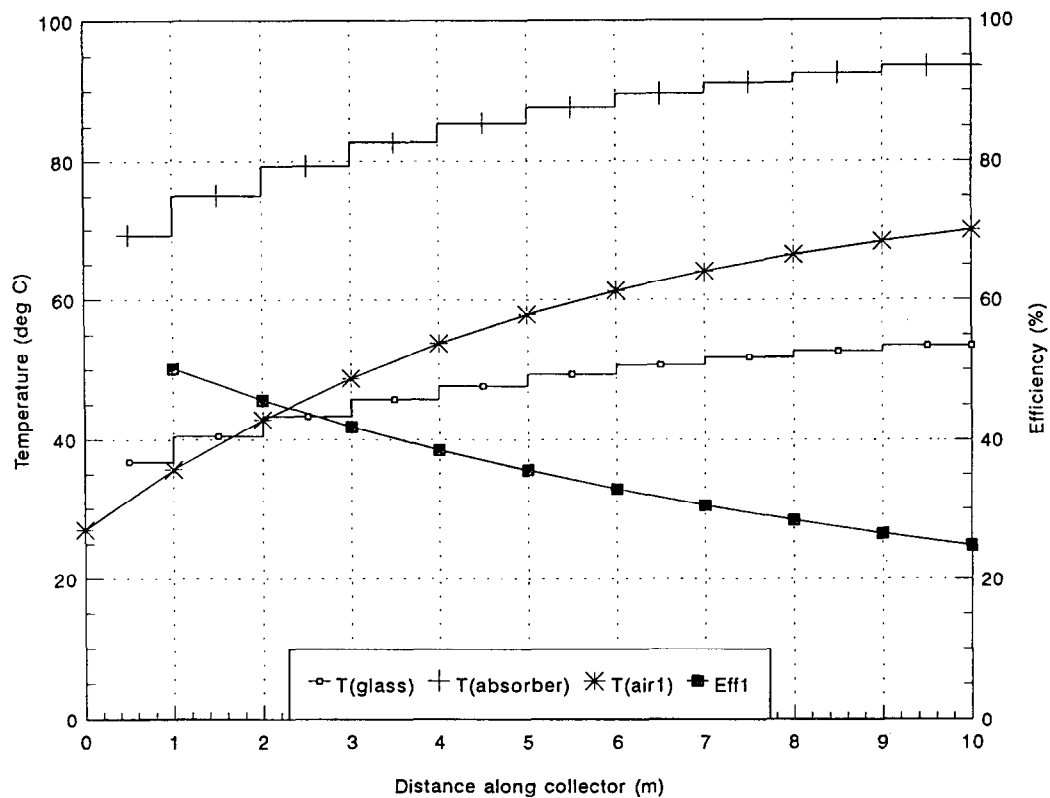


Fig. 7. Theoretical temperature variation along collector for Type I collector at Reynolds Number = 4000.

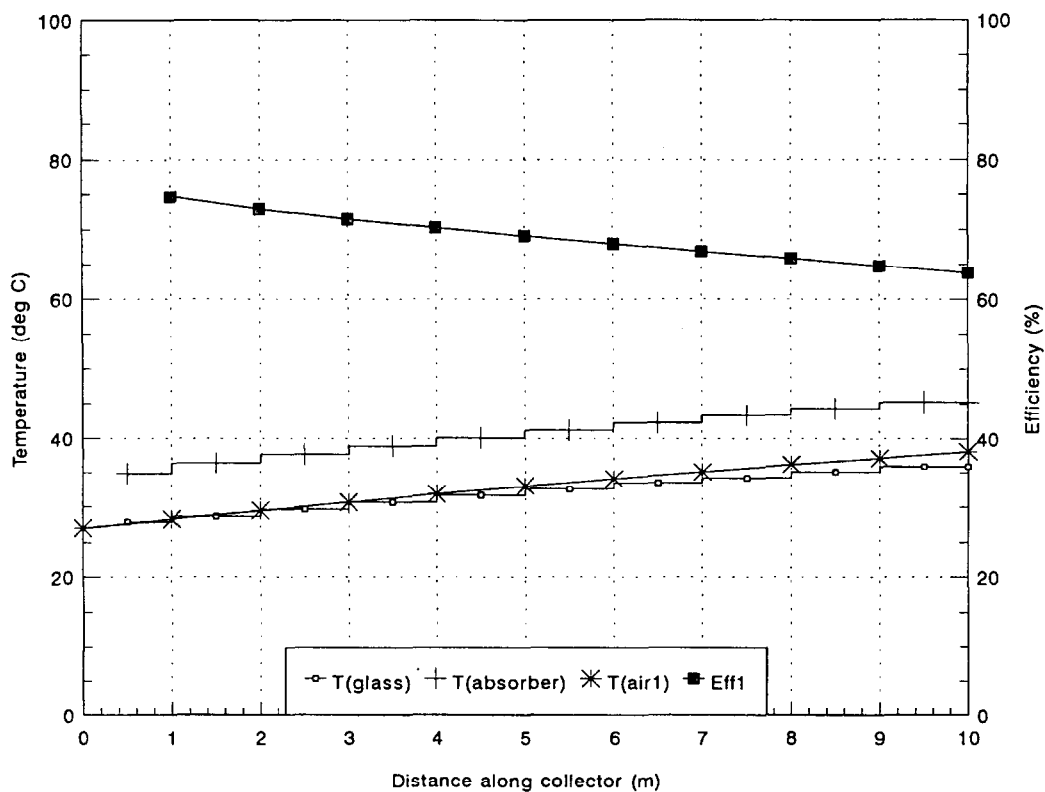


Fig. 8. Theoretical temperature variation along collector for Type I collector at Reynolds Number = 40,000.

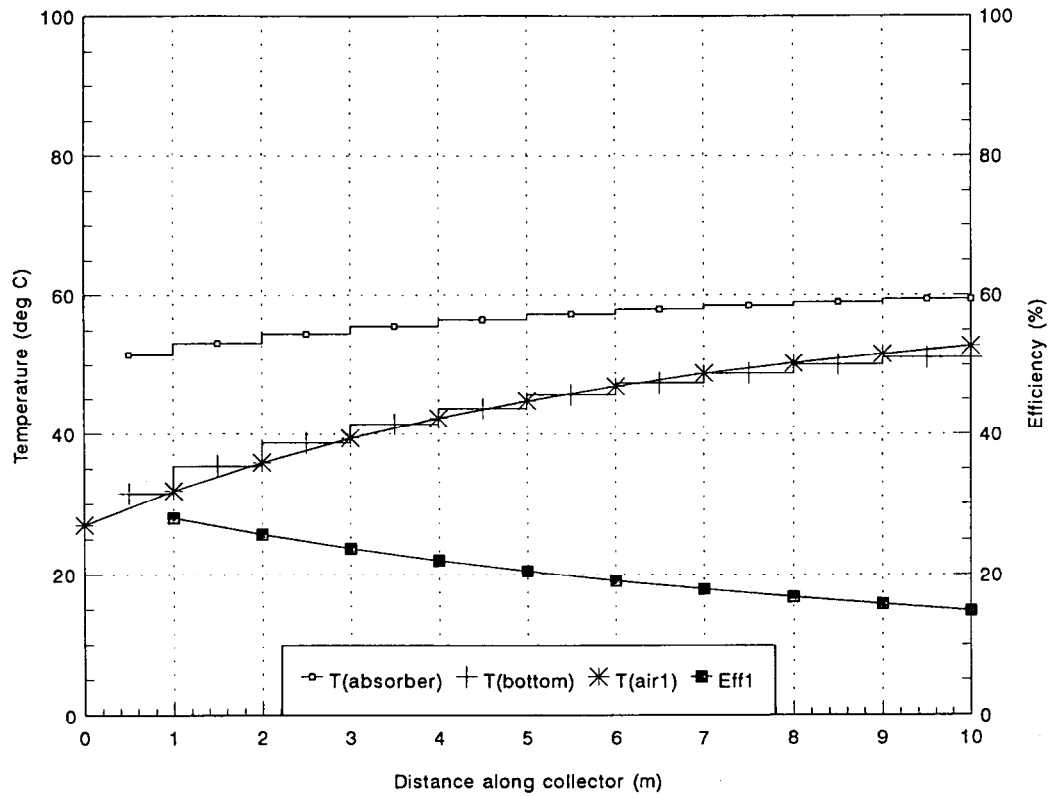


Fig. 9. Theoretical temperature variation along collector for Type II collector at Reynolds Number = 4000.

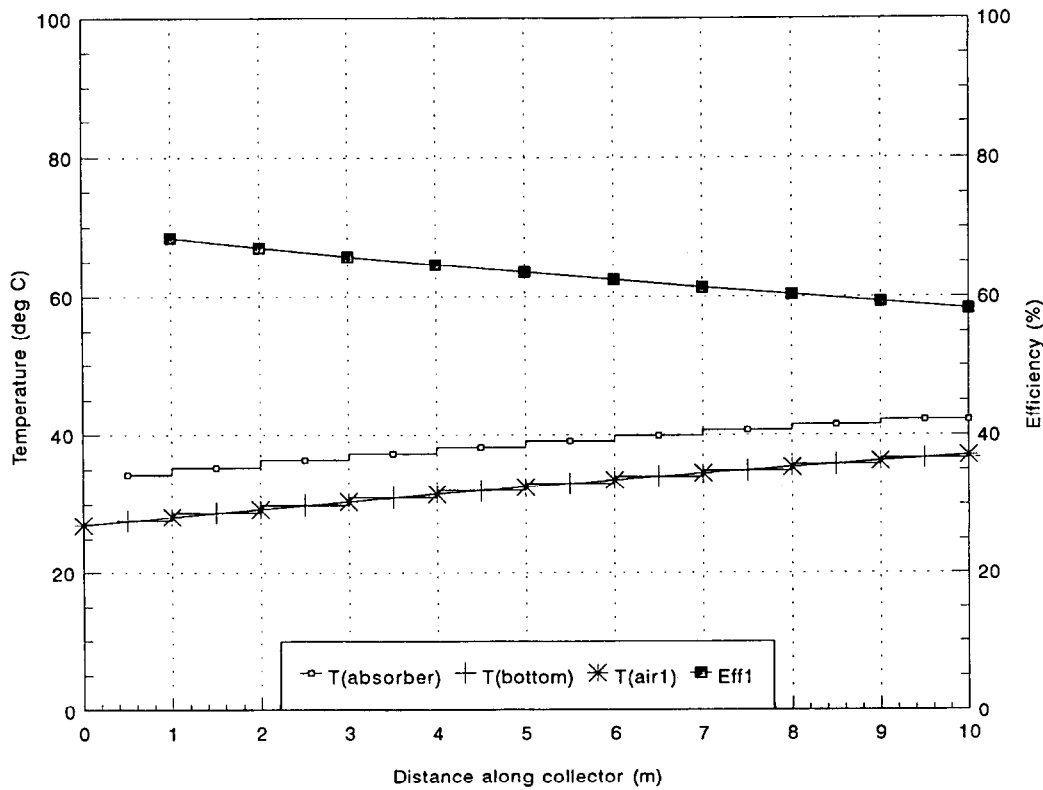


Fig. 10. Theoretical temperature variation along collector for Type II collector at Reynolds Number = 40,000.

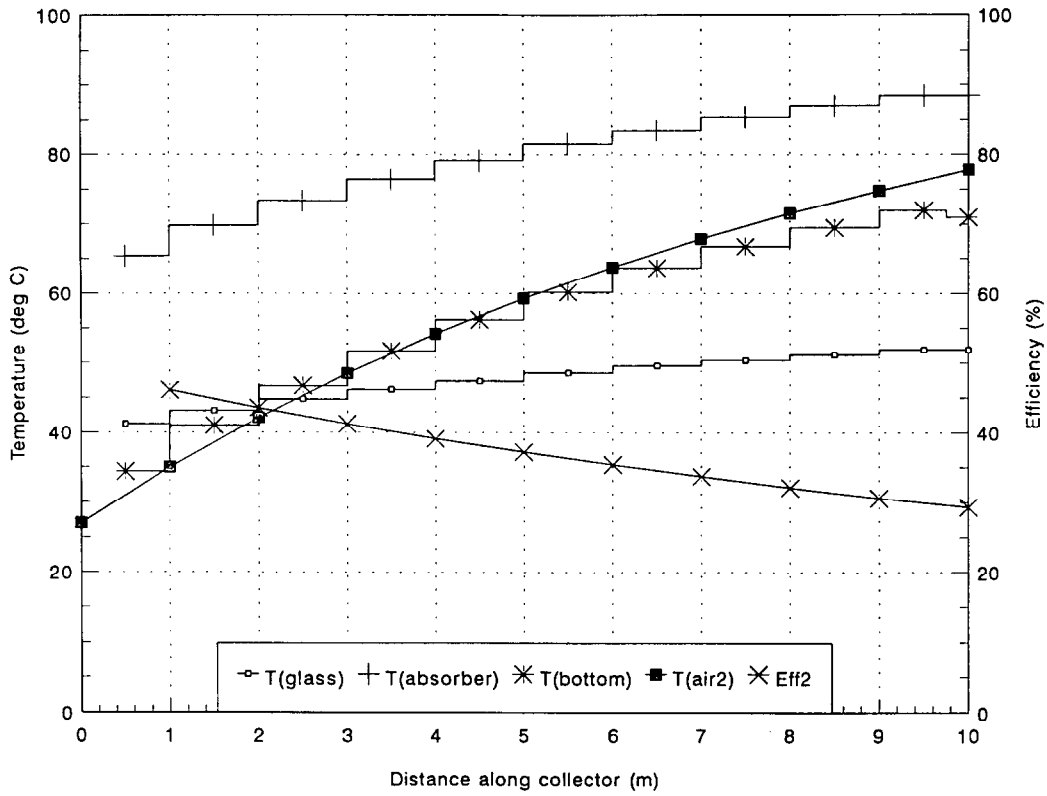


Fig. 11. Theoretical temperature variation along collector for Type III collector at Reynolds Number = 4000.

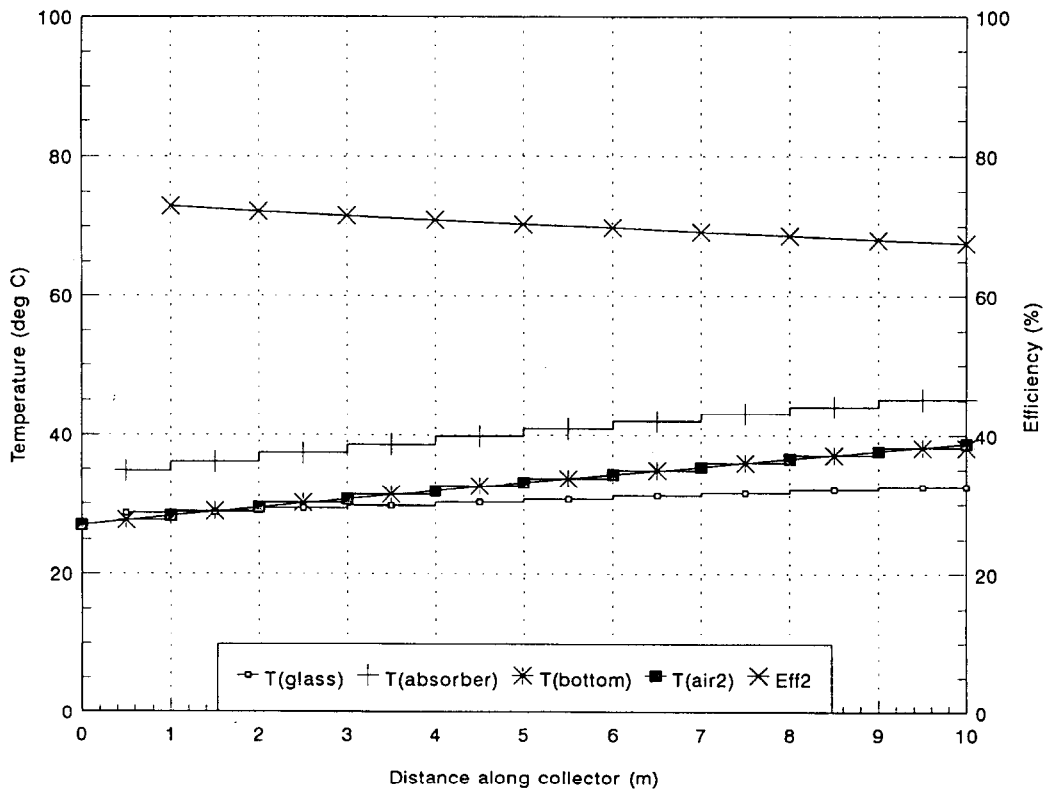


Fig. 12. Theoretical temperature variation along collector for Type III collector at Reynolds Number = 40,000.

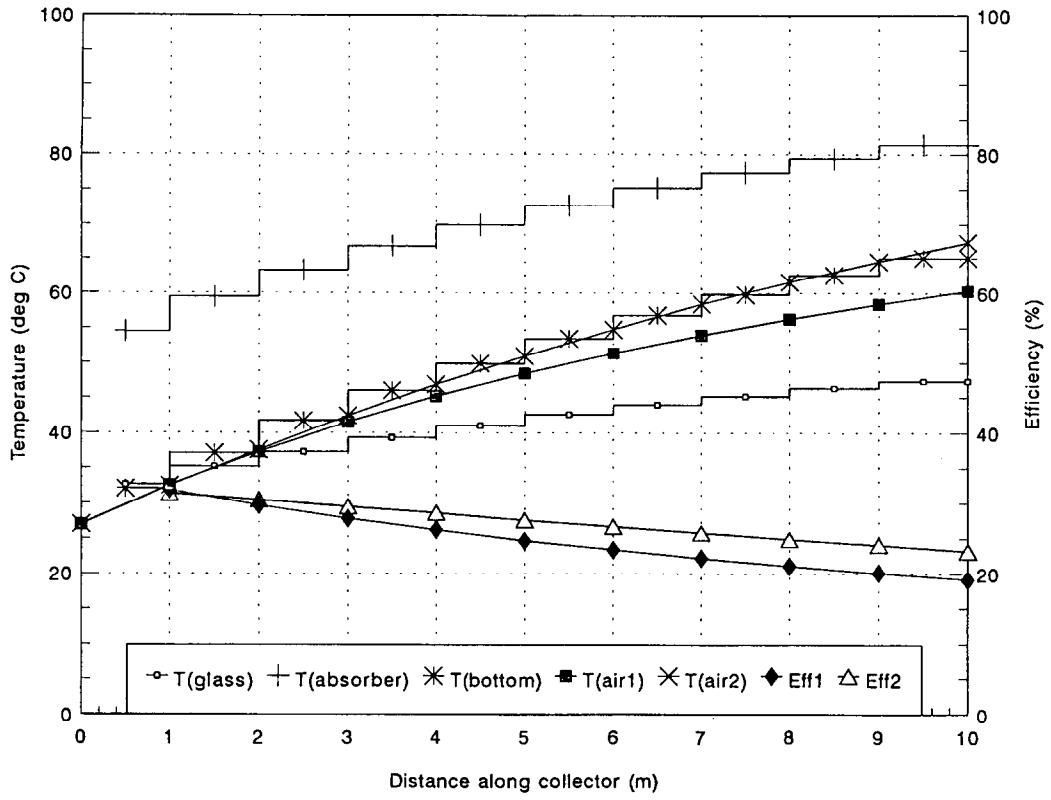


Fig. 13. Theoretical temperature variation along collector for Type IV collector at Reynolds Number = 4000.

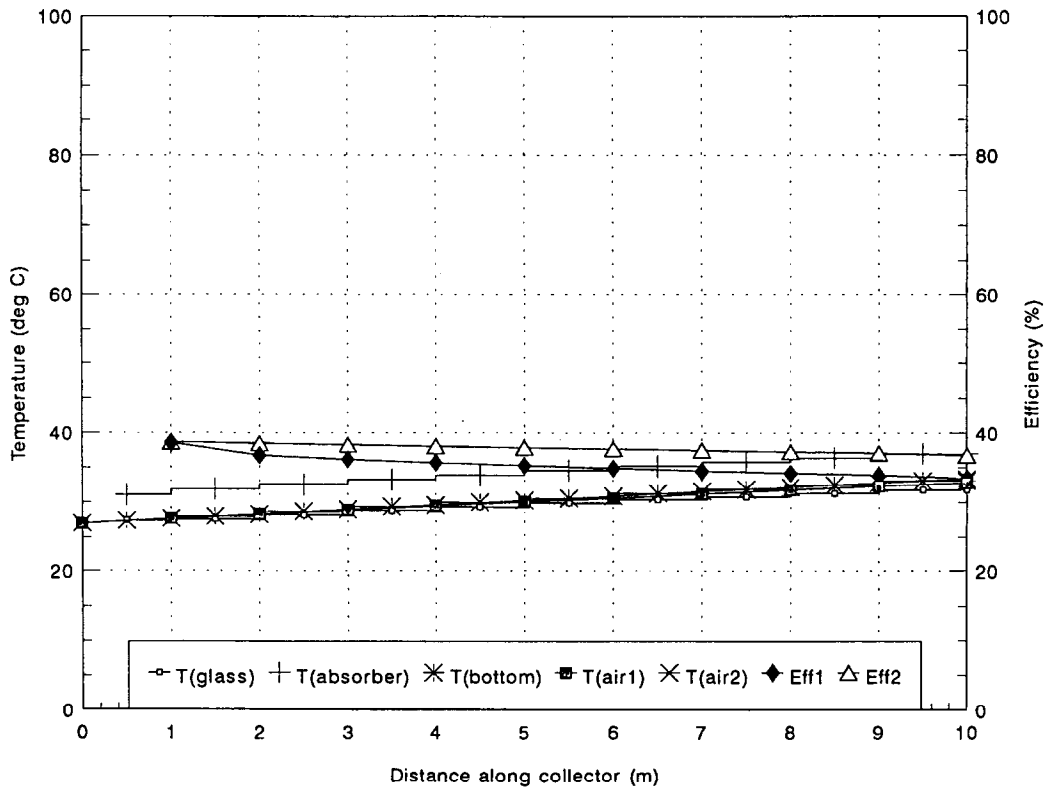


Fig. 14. Theoretical temperature variation along collector for Type IV collector at Reynolds Number = 40,000.

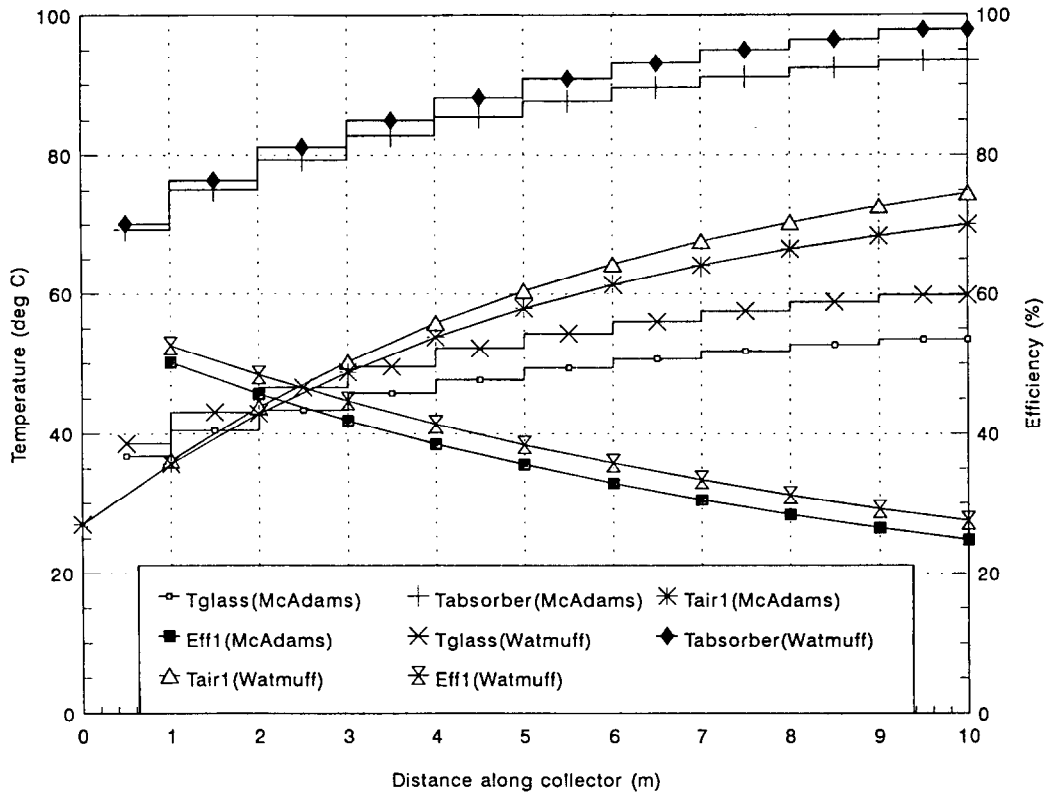


Fig. 15. Effects of wind heat transfer coefficient for Type I collector at Reynolds Number = 4000.

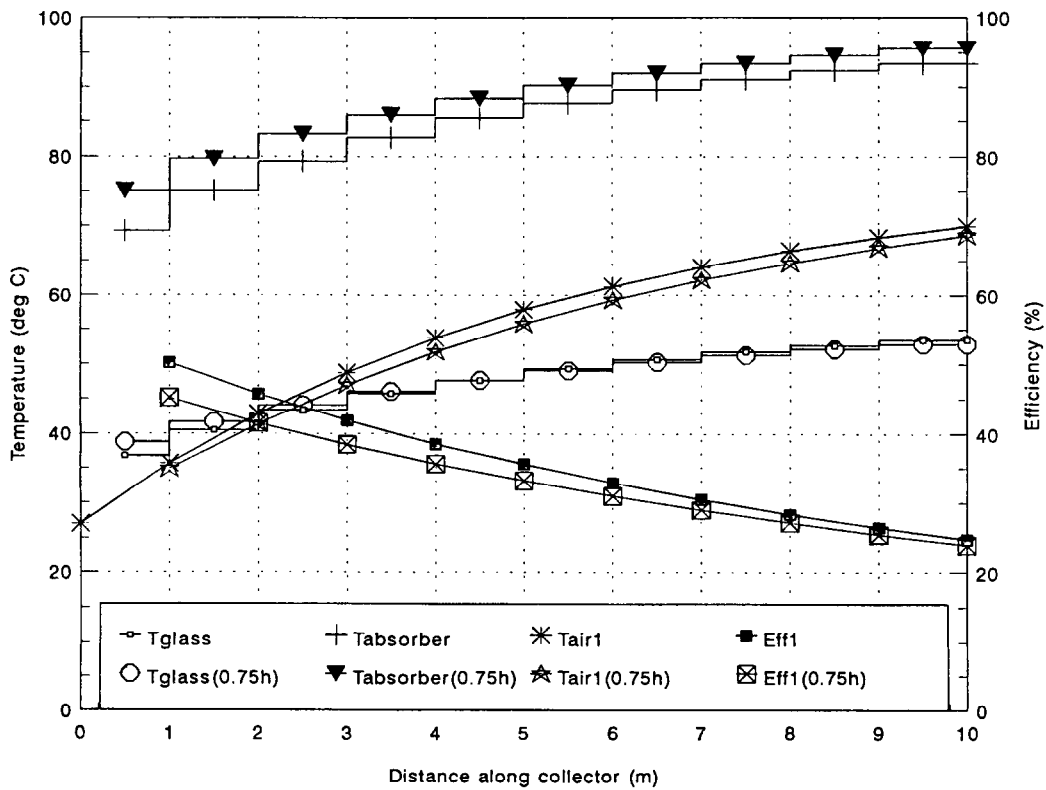


Fig. 16. Effects of film heat transfer coefficients for Type I collector at Reynolds Number = 4000.

about  $10.5 \text{ W m}^{-2} \text{ K}^{-1}$ . From Table 1, the wind heat transfer coefficients  $h_w$  from the different authors varied from  $3.0$  to  $7.6 \text{ W m}^{-2} \text{ K}^{-1}$  at a typical wind speed of  $0.5 \text{ m s}^{-1}$ . The overall top heat loss  $U_t$  is, thus, appreciably affected by the evaluation of  $h_w$ . The effects of the wind heat transfer coefficient on the predicted temperature results are shown in Fig. 15. Two sets of results for the Type I collector at a Reynolds Number equal to 4000 are compared here. The first set evaluates  $h_w$  based on the McAdams (1954) correlation whereas the second set is based on Watmuff *et al.* (1982) correlation. The results show that by decreasing the value of the wind heat transfer coefficient, and thus of the overall top heat loss coefficient value, surface and air temperatures are appreciably increased.

Typical rear insulation for a  $0.025 \text{ mm}$  thick polystyrene sheet ( $k = 0.04 \text{ W m}^{-1} \text{ K}^{-1}$ ) is about  $1.6 \text{ W m}^{-2} \text{ K}^{-1}$ . Combined with the wind coefficient, the overall back loss coefficient is not substantial and would not have any appreciable effect on the predicted results.

#### 5.4. Effects of air-wall convective heat transfer coefficients

In order to demonstrate the effects of the film convective heat transfer coefficients on the overall results, two sets of predictions were obtained for the Type I collector at Reynolds Number equal to 4000. The correlations listed in Table 3 were employed in one set and in the other, the resulting value of the heat transfer coefficients for the air stream was multiplied by a factor of 0.75. The predictions, plotted in Fig. 16 shows that, as expected, lower coefficients resulted in a decreased cooling effect on the absorber plate which resulted in higher plate temperature and lower air stream temperature and thus lower efficiency. The effect on the bottom plate temperature was not so strong as for the others.

## 6. CONCLUSIONS

This paper presents a theoretical model for predicting the thermal performance of flat-plate solar air collectors without recourse to deriving complicated equations. The mathematical solution procedure involved a matrix inversion of the mean temperature vector derived from the energy equations. Predicted temperatures for four types of solar air heaters were presented.

The effects of wind and film heat transfer coefficients on the prediction were discussed.

## NOMENCLATURE

$A_c$	cross section of flow area ( $\text{m}^2$ )
$C$	specific heat of air ( $1009.0 \text{ J kg}^{-1} \text{ K}^{-1}$ )
$D_h$	equivalent diameter, $4 \times$ flow area/wetted perimeter (m)
$D_{h1,h2}$	equivalent diameter of channels 1 and 2 (m)
$f$	friction factor
$g$	gravitational constant ( $9.81 \text{ m s}^{-2}$ )
$h_{1,2,3,4}$	forced convection heat transfer coefficients ( $\text{W m}^{-2} \text{ K}^{-1}$ )
$h_{nc}$	natural convection heat transfer coefficient ( $\text{W m}^{-2} \text{ K}^{-1}$ )
$h_{rb}$	bottom plate—ambient radiation heat transfer coefficient ( $\text{W m}^{-2} \text{ K}^{-1}$ )
$h_{rs}$	top cover—sky radiation heat transfer coefficient ( $\text{W m}^{-2} \text{ K}^{-1}$ )
$h_{r21,r23}$	radiation heat transfer coefficients ( $\text{W m}^{-2} \text{ K}^{-1}$ )
$h_w$	wind convection heat transfer coefficient ( $\text{W m}^{-2} \text{ K}^{-1}$ )
$H$	incident solar radiation intensity ( $900 \text{ W m}^{-2}$ )
$k$	thermal conductivity of air ( $\text{W m}^{-1} \text{ K}^{-1}$ )
$k_{b1,b2}$	insulation thermal conductivity ( $0.04 \text{ W m}^{-1} \text{ K}^{-1}$ )
$L$	length of collector (m)
$m_{1,2}$	mass flow rate of air streams 1 and 2 ( $\text{kg s}^{-1}$ )
$P$	wetted perimeter (m)
$Q_{1,2}$	heat transferred to air streams 1 and 2 ( $\text{W m}^{-2}$ )
$S$	factor in average Nusselt No. evaluation
$S_{1,2}$	solar radiation absorbed by surfaces 1 and 2 ( $\text{W m}^{-2}$ )
$t_1$	spacing between glass and absorber surfaces ( $0.0254 \text{ m}$ )
$t_2$	spacing between absorber and bottom surfaces ( $0.0254 \text{ m}$ )
$T_{1,2,3}$	temperatures of surfaces 1, 2 and 3 (K)
$T_a$	ambient temperature (K)
$T_{f1,f2}$	mean fluid temperatures (K)
$T_s$	sky temperature (K)
$T_{fi}$	mean fluid temperature at inlet to section (K)
$T_{fo}$	mean fluid temperature at outlet of section (K)
$U_b$	bottom heat loss coefficient ( $\text{W m}^{-2} \text{ K}^{-1}$ )
$U_t$	top loss heat coefficient ( $\text{W m}^{-2} \text{ K}^{-1}$ )
$V$	wind velocity ( $1.0 \text{ m s}^{-1}$ )
$W$	width of collector ( $0.254 \text{ m}$ )
$x_{b1,b2}$	insulation thickness ( $0.025 \text{ m}$ )
$y$	distance along collector in flow direction (m)

#### Greek symbols

$\alpha_1$	absorptivity of glass (0.06)
$\alpha_2$	absorptivity of black absorber upper surface (0.95)
$\beta$	volumetric coefficient of expansion [ $2/(T_1 + T_2) \text{ K}^{-1}$ ]
$\Delta T$	temperature difference between plates [ $\text{abs}(T_2 - T_1) \text{ K}$ ]
$\epsilon_1$	emissivity of top glass surface (0.90)
$\epsilon_2$	emissivity of black absorber upper surface (0.95)
$\epsilon_3$	emissivity of unpainted absorber lower surface (0.25)
$\epsilon_4$	emissivity of unpainted bottom plate surface (0.25)
$\eta_1, \eta_2$	efficiency of individual air stream (%)
$\eta_0$	efficiency of combined air streams (%)
$\sigma$	Stefan-Boltzmann constant ( $5.67 \times 10^{-8} \text{ W m}^{-2} \text{ K}^{-4}$ )
$\mu$	dynamic viscosity of air ( $\text{kg m}^{-1} \text{ s}^{-1}$ )
$\phi$	tilt angle ( $75^\circ$ )
$\rho$	density of air ( $\text{kg m}^{-3}$ )
$\tau$	transmissivity of glass (0.84)

## REFERENCES

- Biondi P., Cicala L. and Farina G. Performance analysis of solar air heaters of conventional design. *Solar Energy* **41**, 101–107 (1988).
- Duffie A. D. and Beckman W. A., *Solar Engineering of Thermal Processes*, 2nd edn, Wiley, New York (1991).
- Hausen H., Darstellung des warmenüberganges in rohren durch verallgemeinerte potenzbeziehungen, *VDIZ* **4**, 91–98 (1943).
- Heaton H. S., Reynolds W. C. and Kays W. M. Heat transfer in annular passages, simultaneous development of velocity and temperature fields in laminar flow, *Int. J. Heat Mass Transfer* **7**, 763 (1964).
- Hollands K. G. T., Unny T. E., Raithby G. R. and Konicek L. Free convective heat transfer across inclined air layers, *Trans. ASME, J. Heat Transfer* **98**, 189–193 (1976).
- McAdams W. H., *Heat Transmission*, 3rd edn. McGraw-Hill, New York (1954).
- Nusselt W., Der wärmeaustausch zwischen wand und wasser im rohr. *Forsch. Geb. Ingenieurwes* **2**, 309 (1931).
- Parker B. F., Derivation of efficiency and loss factors for solar air heaters. *Solar Energy* **26**, 27–32 (1981).
- Parker B. F., Lindley M. R., Colliver D. G. and Murphy W. E. Thermal performance of three solar air heaters. *Solar Energy* **51**, 467–479 (1993).
- Petukhov B. S., Heat transfer and friction in turbulent pipe flow with variable physical properties. In *Advances in Heat Transfer*, J. P. Hartnett and T. F. Irvine (Eds), pp. 504–564. Academic Press, New York (1970).
- Sieder E. N. and Tate G. E. Heat transfer and pressure drop of liquids in tubes. *Ind. Engng Chem.* **28**, 1429–1435 (1936).
- Sparrow E. M., Ramsey J. W. and Mass E. A. Effect of finite width on heat transfer and fluid flow about an inclined rectangular plate, *Trans. ASME, J. Heat Transfer* **101**, 2 (1979).
- Swinbank W. C., Long-wave radiation from clear skies, *Q. J. R. Meteorol. Soc.* **89**, 339 (1963).
- Tan H. M. and Charters W. S. Effect of thermal entrance region on turbulent forced-convective heat transfer for an asymmetrically heated rectangular duct with uniform heat flux. *Solar Energy* **12**, 513–516 (1969).
- Tan H. M. and Charters W. S. An experimental investigation of forced-convective heat transfer for fully-developed turbulent flow in a rectangular duct with asymmetric heating. *Solar Energy* **13**, 121–125 (1970).
- Than C. F. and Ong K. S. A theoretical evaluation of a flat-plate solar air heater, *Regional Seminar on Simulation and Design in Solar Energy Applications*, Bangkok (1984).
- Verma R., Chandra R. and Garg H. P. *Optimization of Solar Air Heaters of Different Designs* **2**, 521–531 (1992).
- Vijeyendera N. E., Lee L. A. and Lim E. K. Thermal performance study of two-pass solar air heaters. *Solar Energy* **28**, 363–370 (1982).
- Watmuff J. H., Charters W. W. S. and Proctor D. Solar and wind induced external coefficients for solar collectors. *COMPLES*, No. 2, p. 56 (1977).